Proceedings of the 17th World Congress
The International Federation of Automatic Control
Seoul, Korea, July 6-11, 2008

Experimental autonomous flight of a small-scaled helicopter using accurate dynamics model and low-cost sensors

David Vissière[1] **Pierre-Jean Bristeau**[2]
Alain Pierre Martin[3] **Nicolas Petit**[4]

[1][3] *Délégation Générale pour l'Armement (DGA)*
Laboratoire de Recherches en Balistique et Aérodynamique.
david.vissiere@dga.defense.gouv.fr, alain.martin@dga.defense.gouv.fr
[2] *Ecole Polytechnique, France*
pierre-jean_bristeau@polytechnique.org
[4] *Centre Automatique et Systèmes, Ecole des Mines de Paris, France*
nicolas.petit@ensmp.fr

Abstract: In this paper, we address the problem of guidance and control of a small-scaled helicopter (Benzin Acrobatic from Vario^{TM} with a 1.8 m diameter rotor) equipped with only low-cost sensors. These sensors are an Inertial Measurement Unit (IMU), a GPS, and a barometer, which represent a total cost of USD 3000 including one PC board and one micro-controller). By contrast to other experiments reported in the literature, we do not rely on any accurate IMU or GPS systems which costs are, separately, largely above the mentioned amount of USD 3000. To compensate the weaknesses of this low cost equipment, we put our efforts in obtaining an accurate flight dynamics model. This improves the prediction capabilities of our embedded Kalman filter that serves for data fusion. The main contribution of this paper is to detail, at the light of a successful reported autonomous hovering flight, the derivation of the model. We give numerous details about implementation and discuss the relevance of some modelling hypothesis based on our experience.

Keywords: Low-cost sensors; unmanned vehicle; data fusion; autonomous helicopter; embedded systems; Kalman filter

INTRODUCTION

Numerous military and civilian applications require the use of unmanned vehicles with various degrees of autonomy. Prime examples are Unmanned Air Vehicles (UAV) for borders surveillance, ground attacks, forest fires monitoring, Unmanned Ground Vehicles (UGV) for land mines removal, reach and supply missions, and Unmanned Submarine Vehicle (USV) for deep ocean reconnaissance, or civil engineerings tasks.

The always increasing performance of Micro Electro-Mechanical Systems (MEMS) inertial measurement unit (IMU), and low cost GPS have given them roles of enabling technologies for new autonomous vehicle applications. Yet, challenges are numerous. In particular, down-scaling of helicopters appears very difficult. In this field, several teams have given answers to certain technology questions related, in particular, to autonomous flight. Among these are the outstanding experiments conducted by Mettler (2003); Mettler et al. (2001, 2000b,a), Abbeel et al. (2007); Ng et al. (2004). A R-max helicopter (with a 3.5 m rotor) from Yamaha was used at Carnegie Mellon University Mettler (2003). An X-cell was used at Massachusetts Institute of Technology (this model has a 1.7 m rotor) by V. Gavrilets and Feron (2000).

While accurate dynamics models for such helicopters have been known since the work of Mettler et al. (2000b)and V. Gavrilets and Feron (2001), in all these reported experiments, classic filtering methodology was used. In details, a very general 6 degrees of freedom (DOF) rigid-body model was considered and was reported to be sufficient in coordination with good quality sensors. The reason for this is that the sensors considered in these studies provide accurate enough information for navigation and control. An accurate model was only used for control purposes, which include design, tuning, and simulation.

In this paper, we focus on really low-cost sensors. These sensors belong to the same technology group as those found on the discussed successful experiments, but they are really low-end in their categories. It is believed that cost reduction will yield a substantial speed-up in the spread of UAVs among military and civilian communities. As can be seen from various reported experiments, sensors represent an important part of the total cost of small sized UAVs. This raises some feasibility questions. What are the minimum quality requirements that one must impose on sensors to obtain a navigation system capable of providing real-time information sufficient to feed a stabilizing feedback controller? Which category of sensors can be used for each type of UAV? Which sensor is critical?

Fig. 1. "Goliath", our helicopter equipped with low-cost sensors in hover flight.

We believe that the answer is not solely contained in the sensors specifications. As we wish to demonstrate it, it seems that much improvement can be obtained from the knowledge of UAV models. Rather than considering data fusion algorithms based on a 6 DOF representation of the vehicle under consideration, we think that much attention should be paid to incorporating an accurate flight dynamics model into the data fusion algorithm.

Consider the particular case of small-scaled helicopters. Certainly, it is not possible to include all the equations found in the literature on helicopters. A complexity-accuracy tradeoff must be made. Also, identification of the parameters appearing in the equations can be difficult. At the light of these points, we can reformulate some of the above mentioned questions. What gain can be expected from including a dynamics model of the systems in the data fusion algorithms? Which are the physical phenomena that need to be accounted for and which one can be neglected? These questions (among others in the same spirit) have been partially answered in the case of fixed wing aircraft. We will address them for small-scaled helicopters.

The article is organized as follows. In Section 1, we present our experiment. We detail the helicopter, the sensors under consideration, and their accuracy, and the embedded real-time system. In Section 2, we expose a model for the helicopter. We stress some weaknesses of this approach. In Section 3, we propose modelling improvements and incorporate them in a data fusion algorithm (Kalman filter). Coupling and ground effects are studied. By successively turning off each sensor, we test the robustness of the data fusion algorithm and determine beneficial effect of including the model in prediction phases of the Kalman filter. In Section 4, we conclude and give closed loop results obtained during an autonomous hovering.

1. EXPERIMENTAL SMALL-SCALED HELICOPTER

In this paper, we do not describe the embedded system used to control our small-scaled helicopter in details. These can be accessed through **?**. Yet, its capabilities are presented, to sketch the onboard computational power which can be used to estimate the helicopter state variables. During the design of this embedded system, it was necessary to do a tradeoff between power and weight. Our real-time system uses a Pentium IV (mobile) board for computation and a micro-controller for sensors and actuators interface.

1.1 Aerial vehicle

A versatile hobby helicopter, the Benzin Acrobatic by Vario^{TM} was chosen because of its reliability (we never encountered any mechanical issue during more than 100 flights), its payload capacity (above 5 kg), and its simplicity of servicing. The rotor is 1.8 m wide, and the total mass of the helicopter is 7 Kg (not counting the embedded system). The system is powered by a Zenoah^{TM} 23 cm^3 petrol engine which delivers 2000 W. Once fully loaded with our embedded system (which weights approximately 1.8 Kg), 20 cl of petrol approximately provide 20 min of flight.

1.2 Onboard sensors

In the context of our study, we only considered (low-end) low-cost sensors. We now detail these. In each case, we specify the weight (in g), the cost (in USD), the dimensions (in mm), the update rate (f in Hz), and the protocol of communication (Comm.)

- **Inertial Measurement Unit (IMU)** Our IMU is a 3DM-GX1 from Microstrain^{TM}. It contains three angular rate gyroscope, three orthogonal single-axis magnetometers, and three single-axis accelerometers, along with 16 bits A/D converters and a micro-controller. This IMU can deliver different messages, ranging from raw-data, to reconciliated measurements. In our setup, we ask the IMU to deliver only calibrated sensors data at a 75Hz rate.

Weight	Cost	Size	f	Comm.
30	1450	39,54,18	75	RS232

- **Global Positioning System (GPS):** Our GPS is a TIM-LS from μblox^{TM}. Through a proprietary binary protocol, it provides position and velocity information at a 4Hz rate. Position error is 2.5 m (Circular Error Probability CEP) and velocity error is 2 m CEP.

Weight	Cost	Size	f	Comm.
23	100	32,47,9.5	4	RS232

- **Barometer:** Our barometer is the MS-5534 from Intersema^{TM}. Using a SPI-type protocol, it gives calibrated digital pressure and temperature information.

Weight	Cost	Size	f	Comm.
2	14	5,4,2	20	SPI

- **Take off and Landing detector:** Being able to detect take off and landing instants is necessary to properly initialize data fusion algorithms. In details, detection of the corresponding switches in the dynamics defines when the controls actually have an effect on the system. This is not the case when the helicopter is on the ground. This detection is performed with four on-off switches located at each corned of the landing gear. They deliver a logic signal which can be readily interpreted.

Weight	Cost	Size	f	Comm.
10	6	25,10,5	75	Boolean

1.3 Embedded real-time system

Our (modular) embedded system is composed of a micro-controller, which is in charge of gathering information from all the sensors, and a calculation board. These two

elements are connected by a serial interface. The micro-controller also has a downlink to a ground station. The data acquisition software running on the micro-controller is event-driven by the IMU messages which periodically sends 31 bytes of data. In consequence, the IMU plays a central role among the sensors. Once the message of the IMU is received and validated by the micro-controller, others sensors information are either directly read or picked in data buffers which are constantly fed with serial messages from the sensors through hardware interrupts. Information is gathered in a 116 bytes message containing all the onboard measurements. This message is sent to the calculation board through a high-speed serial port. Once the message is received and validated, the calculation board carries out one navigation loop consisting of a prediction equation and an estimation equation of a Kalman filter. Then, stabilizing closed-loop control values are computed and sent back to the micro-controller which acts upon the servos. This software and hardware architecture has efficient real-time capabilities. We now detail the two discussed constituting elements.

- **Micro-controller** The micro-controller which serves as interface for the sensors and actuators is a MPC555 Power PC from Motorola. It runs a specific software we developed using the Phytec^{TM} development kit. The reason for choosing this micro-controller are as follows. This device provides a double precision floating-point unit (64 bit) which is potentially convenient for embedded algorithms (even if we do not use this possibility here since all computations are performed on the calculation board), it has a relatively fast 40MHz clock, it has 32 bit architecture and 448Kbyte of Flash memory and 4 MBytes of RAM. Most importantly, among the family of 32 bits kits, the MPC555 has substantial computational capabilities and a large of number of versatile and programmable Input/Output ports. In particular we make an extensive use of its TPUs (Time Process Units), UARTs, A/D converters, SPIs, MPIOs (Modular I/O system) (see Motorola (2000)). Finally, it is small (credit card format) and has a low weight.

Weight	Cost	Size	f	Comm.
25	450	72,57,8	all	all

- **Calculation board** The fan-less calculation board we use has a standard PC architecture. Its processor is a 1.2Ghz C7-M from VIA^{TM} designed for embedded applications. It can perform 1500 MIPS and has classic PC Input/Output ports such as a UART serial port (used as main data link with the micro-controller), an ethernet board (not used here), a VGA screen output (which can be used to monitor the system during debugging phases of the software and hardware development), a keyboard, and 4 USB ports (which can be considered for plugging future devices such has controllable cameras). For sake of maximum reliability, this computation board runs a minimal Linux distribution (Knoppix 3.8.1). To maximize performance, we de-activate all hardware interruptions associated to unnecessary devices. Only interrupts from the UART are enabled. A specific UART driver was rewritten for that reason. The operating system is installed on a 1 Gbyte Disk-On-Chip system which prevents all possible mechanical failure associated to hard-drives.

Weight	Cost	Size	f	Comm.
800	350	170,180,40	1.5e6	RS232

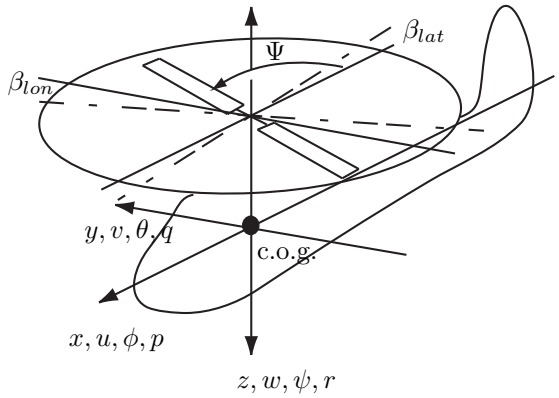

Fig. 2. Notations in the body frame.

2. SMALL-SCALED HELICOPTER MODELLING

In this section, we recall the fundamentals of small-scaled helicopter modelling. We refer to Mettler (2003),for further details.

2.1 Rigid-body model

Frame in use A body reference fixed frame with origin at the center of gravity of the helicopter is considered. The x, y and z axis coincide with the helicopter axis. These axes also coincide with the IMU inner sensors axis. In the following, subscript $_b$ refers to this body frame. As inertial reference frame, we consider the North-East-Down (NED). The X axis is tangent to the geoid and is pointing to the north, the Z axis is pointing to the center of the earth, and the Y axis is tangent to the geoid and is pointing to the East. Subscript $_i$ refers to this inertial frame.

6 DOF rigid body dynamics From a dynamical system point of view, the state of the rigid body is described by the 12 following independent variables

- $X = [x \quad y \quad z]^T$ is the (vector) position of the center of gravity of the IMU in the inertial frame
- $V = [u \quad v \quad w]^T$ is the (vector) velocity of the center of gravity of the IMU in the body frame
- $Q = [\phi \quad \theta \quad \psi]^T$ are the Euler angles, i.e. the angles between the inertial frame and the body
- $\Omega = [p \quad q \quad r]^T$ are the angular rates of turn in the body frame.

The inputs are the forces F and the torques Γ. These inputs consist of the reaction of the rotor onto the body, the aerodynamic forces acting on the body, and the gravity forces. We note m the mass of the helicopter, and I its inertia matrix. With these notations, the dynamics of the 6 DOF rigid body are

$$\left.\begin{aligned} \dot{X} &= R^T V \\ \dot{V} &= -\Omega \times V + F/m \\ \dot{Q} &= G(\Omega, Q) \\ I\dot{\Omega} &= -\Omega \times I\Omega + \Gamma \end{aligned}\right\} \quad (1)$$

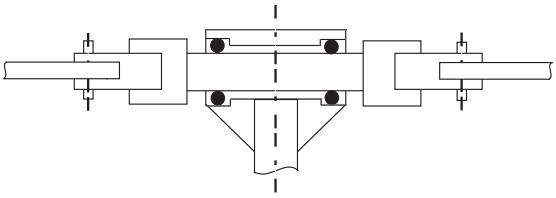

Fig. 3. The particular mechanical structure of the rotor hub enables vertical flapping while preventing the "coning" phenomenon.

with

$$G(\Omega, Q) = \begin{bmatrix} p + (q\sin(\phi) + r\cos(\phi))\tan(\theta) \\ q\cos(\phi) - r\sin(\phi) \\ (q\sin(\phi) + r\cos(\phi))\cos(\theta)^{-1} \end{bmatrix}$$

2.2 Rotor dynamics

One particularity of our helicopter is that a rigid rod connects the two blades of the main rotor (see Figure 2.2). This features rules out any possibility of "coning effect". This effect, commonly found on full-sized helicopters Padfield (2007); Prouty (2003), has an important impact on the thrust generated by the rotor. Because of the relative rigidity of the mentioned rod, we decide to neglect this phenomenon. Yet, the vertical flapping generate a torque M_β.

Main blades dynamics According to the 3 hypothesis formulated in Mettler (2003)– *i*) the vertical flapping angle is assumed small, *ii*) the angle of attack of each blade is small, *iii*) angular accelerations are negligible compared to the angular rate of turn multiplied by rotation speed– the main rotor blades can be represented by 2 state variable a, and b. These correspond to a first harmonic expansion of the periodic motion of the blades. These two states satisfy coupled linear first order dynamics driven by inputs corresponding to the control variables acting upon the rotor head.

$$\begin{cases} \tau_f \dot{a} + a = -\tau_f q + \dfrac{8}{\gamma\Omega^2}\dfrac{k_\beta}{I_\beta} b + A_{lon}\delta_{lon}^{aug} \\ \tau_f \dot{b} + b = -\tau_f p - \dfrac{8}{\gamma\Omega^2}\dfrac{k_\beta}{I_\beta} a + B_{lat}\delta_{lat}^{aug} \end{cases} \quad (2)$$

where γ is the Lock number, k_β is the flapping hinge restraint spring constant, I_β is the blade moment of inertia about the flapping hinge and $\tau_f > 0$. A_{lon} is the longitudinal stick to cyclic pitch gearings, B_{lat} is the lateral stick to cyclic pitch gearings for the main bar.

Bell bar dynamics Following a similar approach, one can consider two additional states, c and d, corresponding to the Bell bar blades. These satisfy a set of two uncoupled linear first order dynamics driven by inputs corresponding to the control variables acting upon the rotor head.

$$\begin{cases} \tau_s \dot{c} + c = -\tau_s q + C_{lon}\delta_{lon} \\ \tau_s \dot{d} + d = -\tau_s p + D_{lat}\delta_{lat} \end{cases} \quad (3)$$

where C_{lon} is the longitudinal stick to cyclic pitch gearings, D_{lat} is the lateral stick to cyclic pitch gearings for the Bell bar and $\tau_s > 0$. The Bell bar has an effect on the main blades dynamics due to so-called "Bell mixer" mechanism. One can consider that the actual inputs in (2) are "augmented" as follows

$$\begin{cases} \delta_{lat}^{aug} = \delta_{lat} + K_d d, \\ \delta_{lon}^{aug} = \delta_{lon} + K_c c. \end{cases} \quad (4)$$

Additionally, the Bell bar has an impact on the overall response time of the rotor. By adjusting its inertia (and aerodynamics) properties, this time constant can be rendered consistent with the skills of the pilot and its own response time in order to ease its task. This can help and make piloting easier, yet this is not a true stabilizing effect as could be erroneously understood.

Resulting forces and torques on the rigid body The aerodynamics states a, b, c, d presented above can be used to define the orientation of the rotor thrust $\boldsymbol{R_{aero}}$ and the torque $\boldsymbol{M_{aero}}$ acting upon the rigid body of the helicopter. M_β represents the torque corresponding to the spring effect of the rotor hub. Around steady state, these are

$$\begin{aligned} \boldsymbol{R_{aero}} &= T\ [-a,\ b,\ -1]^T \\ \boldsymbol{M_{aero}} &= hT\ [b,\ a,\ 0]^T \\ \boldsymbol{M_\beta} &= k_\beta\ [b,\ a,\ 0]^T \end{aligned} \quad (5)$$

where T is the norm of the thrust generated by the main rotor, and h is the distance between the center of application of the thrust and the center of gravity of the helicopter. Around hovering $T \approx mg$. As will be discussed later on, the thrust is depending on δ_{col} (and on z). More generally, the magnitude of the thrust can not be easily computed. Quantitatively evaluating it requires Computational Fluid Dynamics (CFD) solvers which are usually out of the scope of control-oriented studies. Rather, identification from flight data can be performed and they appear to provide satisfactory results.

2.3 Tail Rotor

To compensate the torque generated by the main rotor, the tail rotor produces a force acting with a large lever arm (0.95 m in our case). This result in a torque M_{tail} which depends on δ_{ped}. This force also induces a lateral acceleration which is cancelled out by a steady inclination of the main rotor. More complicated effects usually appear in practice. In particular, there exists some undesired interactions between the main rotor and the tail rotor through the air fluxes. These effects are always cancelled by a low-level control system consisting of a rate-gyroscope located along the tail which measures r_m and acts upon the angle of attack of the tail rotor δ_{ped}. We identified the response of this control system on our helicopter. It is well represented by a 2 Hz low pass filter on the pilots orders with a feedforward on the tail rate-gyroscope. Later, in filtering equations, we consider that the input to the system is δ_{ped} the output signal of the tail gyroscope.

2.4 Weaknesses of the model

Before we proceed further and incorporate equations (1)-(2)-(3)-(4)-(5) into a data fusion algorithm, it is important that we comment on some of their apparent weaknesses.

Neglected phenomena The model (1)-(2)-(3)-(4)-(5) presented above where the forces and torques are $\boldsymbol{R_{aero}}$

added to the gravity forces and the tail rotor thrust and $\boldsymbol{M_{aero}} + \boldsymbol{M_{\beta}} + \boldsymbol{M_{tail}}$, respectively, is sufficient for state feedback control purposes. This point was raised by Mettler (2003), with extensive supportive experimental results. Yet, when the question is to estimate the attitude and position of the helicopter, it can be useful to account for further details. Among these are ground effet, actuators-induced lags and response time, and aerodynamics effect of the air flow from the main rotor passing by the body of the helicopter (rotor-induced body drag). These points will be developed in Section 3.2.

Parameter identification Another point worth mentioning is that several key parameters must be available to obtain accurate estimates from the model (1)-(2)-(3)-(4)-(5). In particular, the inertia matrix I, and expression of the magnitude of the thrust T as a function of δ_{col} (see Equation (5)) and the tail rotor torque M_{tail} as a function of δ_{ped}, response times of both the main rotor and the Bell bar (τ_f and τ_s in Equation (2) and (3)), as well as k_β, I_β, γ in (2), A_{lon}, B_{lat}, C_{lon}, D_{lat} and the position of the center of gravity are needed. In Section 3.2, we explain how to identify these parameters.

3. MODELLING IMPROVEMENTS AND DATA FUSION

3.1 Filter design and implementation

For state estimation, we use an Extended Kalman Filter which serves as a data fusion algorithm. The state of our filter has a total dimension of 23 in its current version. In details, we use 13 states to represent the 12 (independent) configuration states of our 6 DOF helicopter (quaternions are used to avoid well know singularities at $\theta = \frac{\pi}{2}$), we use 4 states to model the rotor dynamic (as discussed in Section 2.2), we use 6 states to model additional external (unknown) torques and forces. Theses forces and torques represent un-modelled terms, and, most importantly, wind gusts. A first approach can be to assume that these additional unknowns satisfy some first order dynamics driven by white noises ν_F (referring to forces) and ν_Γ (referring to torques). Dynamic noise variance must be taken large enough to capture the neglected dynamics, while the response time is tuned such that F and Γ are consistent with the dynamics while reducing the 25Hz noise due to the main rotor rotation. More generally, performance certainly increases with the size of the state used for filtering, for example sensor drifts can be modeled this way. Limitations of the available computational power suggested us to use only a small number of stated for these unknowns.

The measurement vector sent by the micro-controller to the computation board is composed of multi-rate data. IMU data, barometer data are both updated at a $75Hz$ rate, while and GPS data are updated at a $4Hz$ rate. The filter equations are presented below. In implementation, the covariance matrices can be initialized with values being consistent with the ranges of dynamics under consideration of our system. In details, typical speeds and accelerations are used. The filter updates are synchronized with the 75 Hz IMU measurements. Classically, discrete-time update equations are considered. A special attention is paid to maintain the covariance matrices positive.

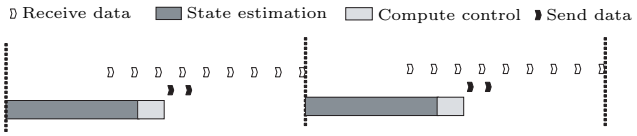

Fig. 4. Succession of steps of data transfer and computation.

Note P_p the 23×23 covariance matrix of the state used for prediction, P_e the 23×23 covariance matrix of the state used for estimation, Q the 23×23 covariance matrix used in the noise dynamics, R_{IMU} the 7×7 covariance matrix considered in the sensor noise definition for IMU and barometer,R_{GPS} the 6×6 covariance matrix considered in the sensor noise definition for GPS position and velocity, X_p the 23 dimensional predicted state, X_e the 23 dimensional estimated state, A the 23×23 matrix of the system obtained by linearizing dynamics (1)-(2)-(3)-(4)-(5), C_{IMU} the 7×23 matrix and C_{GPS} the 6×23 matrix obtained by linearizing the measurement equation, $\dot{X} = F(X, U)$, and T the sample time (between measurements updates).

First, we perform a prediction step from time k to $k+1$, obtaining X_p and P_p. Then, we estimate the state through the measurements to obtain X_e and P_e. The updates are computed as follows

$$
\begin{aligned}
X_p &= X_e + F(X_e, U)T \\
P_p &= (I + AT)P_e(I + AT)^T + QT + (AQ + QA^T)\frac{T^2}{2} \\
&\quad + AQA^T\frac{T^3}{3} \\
Y_p &= [F - \boldsymbol{g} + B_V; \Omega + B_\Omega; M]^T \\
K &= P_p C^T (R + C P_p C^T)^{-}1 \\
X_e &= X_p + K(Y - Y_p) \\
P_e &= (I - KC)P_p(I - KC)^T + KRK^T
\end{aligned}
$$

Where R and C correspond to GPS or IMU depending on the current measurement. According to this, the code embedded into the calculation board is structured as follows

(1) **UART reading:** the UART driver gets the data sent by the micro-controller.
(2) **Message decoding:** once received, the data are transmitted to the user space. These data are composed of 8-bytes word which must be decoded according to the sensor vendors proprietary protocols.
(3) **Initialization:** all the values needed for state estimation are initialized. This also includes white dynamic and sensor noises, constants in use, and reference control values.
(4) **Prediction:** in this step, we use the estimated state $\hat{X}_{e\_k}$ at time T_k to predict the state $\hat{X}_{p\_k+1}$ at time T_{k+1} accounting for the non-linear dynamics and the discrete sampling time T.
(5) **Estimation:** in this step, we use the measurements and the predicted state $\hat{X}_{p\_k+1}$ at time T_k to update the estimated state $\hat{X}_{e\_k+1}$ at time T_{k+1}.

Fig. 5. Three dimensional view of the CATIA® model of our helicopter. 680 different parts are modelled and kinematically linked together. Payload, landing-gear, sensors, electronic devices, Li-Po batteries, and numerous add-ons are modelled to obtain accurate estimates of inertia matrix and position of the center of gravity.

(6) **Control:** new values of the control are computed with, e.g., a state feedback on the estimated state.
(7) **Sending orders:** the UART driver is used (in interrupt mode) to transmit control values back to the micro-controller. In turn, the micro-controllers acts upon the servos.

These tasks are scheduled according to the chart given in Figure 4. The main loop detailed above is executed at a 75 Hz rate (approx. every 13.33 ms). Among the numerous tasks, the filter calculations take approximatively 6 ms, while receiving the data takes about 10 ms (mostly waiting time), and computing and sending back the control values takes 1 ms. An interrupt driven approach much be used to run all these task within the allowed 13.33 ms.

3.2 Details of the prediction step

In this subsection, we wish to expose the numerous details and phenomenon we take into account in the model. In particular, we detail the identification of physical parameters, the effect of the collective pitch and the induced speed, the ground effect, the effect of the tail rotor pitch control, and the effect of the longitudinal and lateral cyclic pitch angles.

Identification of the inertia matrix and the center of gravity As mentioned in Section 2.4.2, we desire, for sake of state estimation accuracy, to have good estimates of the inertia matrix and the position of the center of gravity of our helicopter. For that purpose, we use Dassault Systèmes's CATIA® software. Taking into account their various geometries and densities, 688 different parts were modeled and kinematically linked together. In particular, the basic structure, the engine, the blades, the payload, the landing-gear, the GPS, the power supplies, the Li-Po batteries, and numerous add-ons (such as flat cables or reservoir) were modelled. The obtained information is directly used to compute lever-arms of forces and to correct the IMU and GPS information. It should be noted that, while originally located under the rotor axis, the center of gravity is now 1.9 cm behind it.

Effect of collective pitch angle in vertical climb The vertical displacement of the helicopter is directly impacted

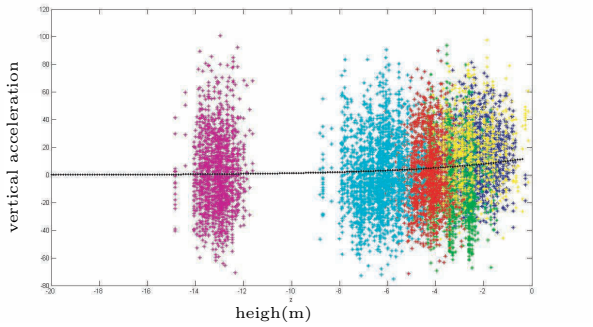

Fig. 6. Ground effect impact on the vertical acceleration.

by the value of θ_0 which stands for the collective angle of attack of the blades (collective pitch angle). For small angles of attack, we can model the magnitude of the generated thrust as a linear function of the mean value of the angle of attack. Linearization around hovering equilibrium values yields

$$T = -mg - Z_{col}(\delta_{col} - Col_s) \tag{6}$$

where Z_{col} can be experimentally obtained as the ratio between the vertical acceleration and the control values δ_{col}, Col_s is the mean value of the control generated by the pilot for a stationary hovering flight in a flight zone where the ground effect is negligible. It can be noticed that $Z_{col}Col_s$ is greater than the gravity due to the compensation of Col_i which represents the reduction of the angle of attack due to the rotor induced velocity. In practice, the control δ_{col} is directly measured by the micro-controller which captures the signal sent to the servos. The fit quality of the proposed affine law can be checked in Figure 3.2.5).

Ground effect Experimentally, substantial errors of the preceding model (6) are observed when the helicopter flies at low altitude. This phenomenon is a ground effect for which we propose to introduce corrective terms in (6). Generally, a helicopter flying close to the ground requires less power than when it is flying far from it. Numerous models have been proposed in the literature for this phenomenon seen on various aircrafts. For helicopters, Rozhdestvensky (2000) has proposed a ground effect theory appearing when the altitude is less than the chordwise length. In this approach, an additional thrust inversely proportional to the high is considered. Separately, Lefort and Hamann (1988) propose another point of view, and model the induced speed as being inversely proportional to the square of the distance between the rotor hub and the ground, when the altitude is less than one length of blade. Here, we simply use an exponentially decaying model which fits the experimental results well. This model is

$$T = -mg - Z_{col}\left(\delta_{col} - Col_s + Col_{GE}\exp\left(\frac{z}{Z_{GE}}\right)\right) \tag{7}$$

where Col_s equals the value of the control signal sent to maintain a stationary flight when the ground effect is negligible. Parameters Col_{GE} and Z_{GE} are positive. Their values were experimentally obtained during some long time hovering flights at various altitude. In Figure 3.2.3, we present un-filtered signals which permit to estimate

these parameters. Accelerometers noises are at the birth of the large variance of the data. The fitted exponential law is depicted in black. We obtain $Z_{GE} = 0.5m$ which equals one main blade length, and $Col_{GE} = 180$, $Col_S = 610$. The additional acceleration due to ground effect is around $\frac{g}{3}$ on ground. Those value are consistent with the orders of magnitude of our helicopter.

Impact of the tail rotor pitch angle on the yaw motion

The tail rotor pitch angle δ_{ped} is the control signal sent to the tail rotor servo. Due to the affine relation between the actual control (PWM signal) and the obtained angle of attack (see Figure 3.2.5), the resulting force is of the form $Y_{ped}\ \delta_{ped}$, where $Y_{ped} > 0$. Using the experimentally obtained values of the acceleration of the helicopter along the y-axis, we compute Y_{ped}. Then, we evaluate the resulting torque under the form $N_{ped}\ \delta_{ped}$ at the center of gravity by taking into account the mass and lever harm L_{ped}. This yields

$$N_{ped} = -L_{ped}\ m\ Y_{ped}.$$

In the absence of yaw variation, δ_{ped} is such that the torque due to the tail rotor thrust and the torque generated by the main blade cancel each other. During a stationary flight, The mean value for δ_{ped}, noted δ_{peds}, provides us with an estimate for the aerodynamic moment. The influence of the tail rotor on the helicopter dynamics is as follows. It generates a y-axis force F_{tail} and impacts on the rotational dynamics along the r axis by a torque $M_{tail} = N_{ped}\delta_{ped}$. In details, one obtains

$$\begin{cases} F_{tail} = Y_{ped}\ \delta_{ped}, \\ I_{ZZ}\dot{r} = N_{ped}(\delta_{ped} - \delta_{peds}). \end{cases}$$

where I_{ZZ} is the third diagonal term of the inertia matrix I. Modelling improvements could include the impact of a variation of collective pitch angle δ_{col} onto the aerodynamic moment (when δ_{col} increases, the aerodynamic moment on main blade also increases which explains why the engine throttle control is statically coupled to δ_{col} in order to keep a constant angular velocity for the rotor hub). This would imply that δ_{peds} is in fact a function of δ_{col}. Theoretically, this coupling could be identified online but it appears to be very difficult to estimate due to the high noise/signal ratio of the yaw gyroscope of our IMU. Therefore, we neglect this phenomenon.

Effects of the the longitudinal and lateral cyclic pitch angle onto the horizontal motion of the helicopter

Flapping dynamic According to equation (2) and (3), the dynamics of the rotor hub are as follows

$$\begin{cases} \Theta(\Psi) = \Theta_0 - B_{lat}(\delta_{lat} + K_d d)\cos\Psi \\ \qquad\qquad + A_{lon}(\delta_{lon} + K_c c)\sin\Psi, \\ \tilde{\Theta}(\Psi) = \Theta_0 - D_{lat}\delta_{lat}\cos\Psi + C_{lon}\delta_{lon}\sin\Psi \end{cases} \tag{8}$$

where $\Theta(\Psi)$ (resp $\tilde{\Theta}(\Psi)$)is the blade pitch angle for the main bar (resp for the Bell bar) which depends on Ψ the blade azimuth angle. Its formal harmonic decomposition, through the c and d variable in particular, can be used in identification experiments to derive K_c, K_d, A_{lon}, B_{lat}, C_{lon}, and D_{lat}.In equation (8) collectif pitch angle θ_0 depends on δ_{col}. Interestingly, these experiments can be carried out under rest conditions, and need not in-flight data.

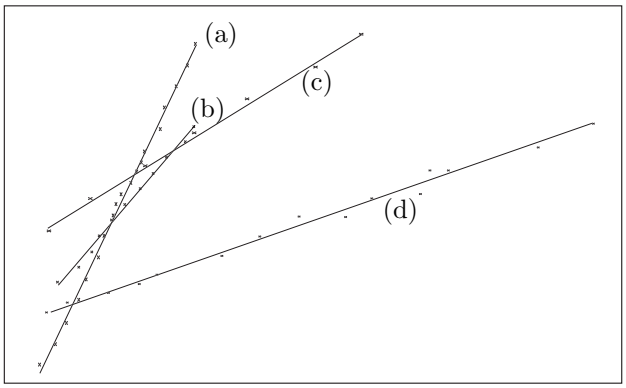

Fig. 7. Affine relation between (a) δ_{lon} and $\tilde{\theta}$, (b) δ_{lon} and θ,(c) δ_{col} and θ_0, (d) δ_{ped} and pitch angle for tail rotor.

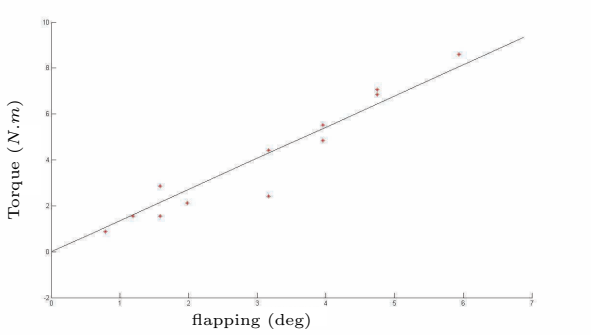

Fig. 8. M_β as a function of the flapping.

The static gains A_{lon}, B_{lat}, C_{lon} and D_{lat} play a role in the main rotor and the Bell bar. The control variables δ_{lon} and δ_{lat} are such that their zero values correspond to a null angle of attack of the blade (without taking into account collective angle of attack). The static gain C_{lon} (resp D_{lat}) is the gain between cyclic controls and the pitch angle of Bell bar. It is directly measured by aligning the Bell bar with the lateral axis (resp longitudinal axis), see Figure 3.2.5(a). Similarly, A_{lon} (resp. B_{lat}) was experimentally obtained while keeping the Bell bar horizontal, see Figure 3.2.5.

The amplifying effect of the Bell bar on control variables is characterized by the two gains $AC = A_{lon}K_c$ and $BD = B_{lat}K_d$. Those two gains were measured as the ratio between the angle of attack of the Bell bar and the main bar, for various values of c and d see Figure 3.2.5. The rotor hub spring constant k_β was obtained by attaching masses on main blade and measuring the return torque as a function of flapping of the main bar see Figure 8). The gain $AB = \frac{8}{\gamma\Omega^2}\frac{k_\beta}{I_\beta}$ may be computed vias the value of I_β (obtained via CATIA)

Forces and torques balance Using a detailed expression of $\boldsymbol{R_{aero}}$, Equation (5) yields

$$\boldsymbol{R_{aero}} = (g + Z_{col}(\delta_{col} - Col_s + Col_{GE}\exp\frac{z}{Z_{GE}}))\begin{bmatrix} -a \\ b \\ -1 \end{bmatrix} \tag{9}$$

A lever arm is used to compute the aerodynamic moment

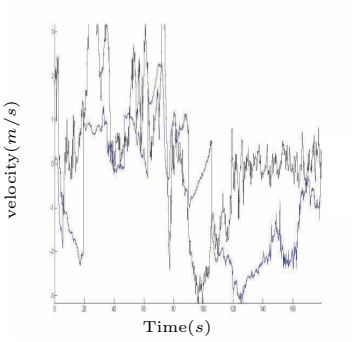

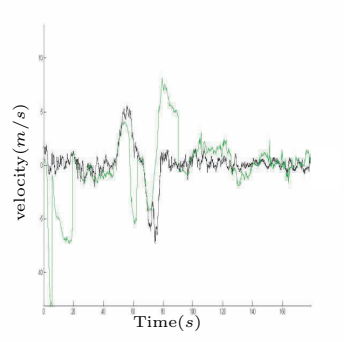

Fig. 9. Longitudinal velocity $u(m/s)$ (blue) and lateral velocity $v(m/s)$ (green) estimated and measured by GPS (black). Flight time (s) is reported on the x-axis.

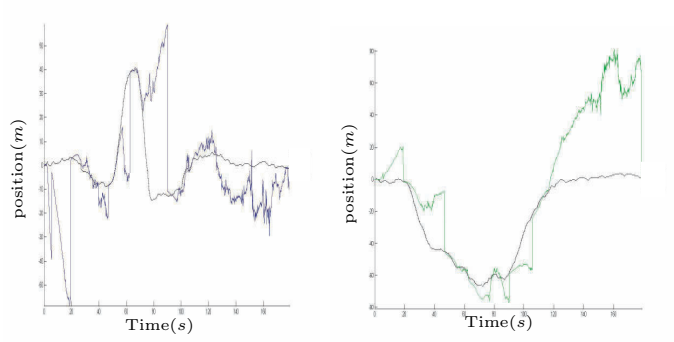

Fig. 10. Position: estimated along x-axis (blue) and y-axis (green), and measured by GPS (black). Flight time (s) is on the x-axis.

$$\boldsymbol{M_{aero}} = M(g + Z_{col}(\delta_{col} - Col_s + Col_{GE} \exp \frac{z}{Z_{GE}})) \begin{bmatrix} -Z_{aero}\ b \\ -Z_{aero}\ a + X_{aero} \\ X_{aero}\ b \end{bmatrix} \quad (10)$$

The torque due to the rotor hub spring effet is given by

$$\boldsymbol{M_\beta} = k_\beta \begin{bmatrix} b & a & 0 \end{bmatrix}^T \quad (11)$$

3.3 Experimental estimation results

In this section, we present experimental state estimation results obtained onboard our helicopter. We study the robustness by successively turning on and off every sensor.

Robustness, accuracy of the model, and sensors failure We successively turn off the GPS velocity and position information, and the gyrometer angular rate of turn signal.

- **Loss of GPS:** to simulate a GPS loss during a flight, and to evaluate the relevance of the linear dynamic model as a substitute, we turn off the 4 Hz measurement and run the data fusion Kalman filter with only 0.5Hz measurement, see Figure 9 and Figure 10. The flight under consideration is a typical forward flight at average speed. The value of Euler angle are lightly disturbed. Position and velocity are strongly updated when a new measure appears, but, interestingly, some parts of the flight are well predicted. In particular, the position estimates are relevant.
- **Gyrometer failure:** to test the relevance of the model with respect to the angular dynamics, we turn off the gyroscopes. Position and velocity errors remain large but do not grow unbounded, while angle estimates are debased. Yet, the predicted angular rate are really close to their real values, as can be seen in Figure 11. In turn, the torques are well estimated. This point is consistent with the well predicted variations of the roll/pitch angles which can be seen in Figure 11. These track the reference values obtained from the internal 6 DOF rigid-body state estimation algorithm IMU (which we do not use otherwise).
- **Barometer failure:** to test the ground effect model, all sensors except barometer were turned on. Results are presented in Figure 12).

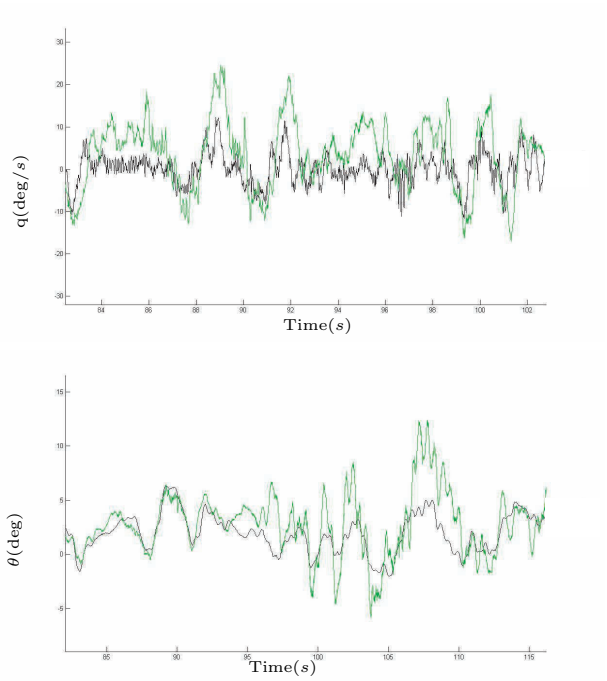

Fig. 11. Angular velocity p: (deg $/s$) estimated (green) and given from the IMU (black). Pitch angle θ(deg): estimated (green) and given by the IMU filter (black). Flight time (s) is reported on the x-axis.

The estimated altitude relies on model exclusively (vertical accelerometer is too noisy to expect to yield reasonable estimates). The variance of altitude error is 3.5 m which is quite good. Altitude is always negative which is also good.

Remaining weaknesses It appears that modelling of drag remains the source of non-negligible uncertainties. Also, masking effects between the two rotors seem a problem when the helicopter is moving. We hope to be able to get more insight on these points soon.

4. CONCLUSION

In this paper, we focused on incorporating important details in the flight dynamics used for data fusion onboard an experimental small-scaled helicopter. Estimation results

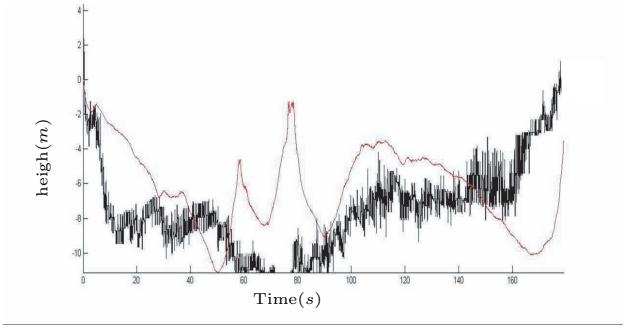

Fig. 12. Altitude: estimated (blue) and measured by the barometer (black). Flight time (s) is reported on x-axis.

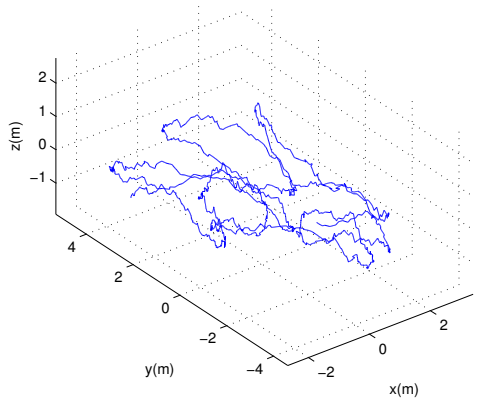

Fig. 13. Autonomous stationary flight. Position errors.

prove the relevance of the approach which relies solely on low-cost sensors. Eventually, we used this real-time estimated state vector in a feedback controller. Classically, because of the substantial coupling terms in this multi-variable dynamics (see Balas (2003)), a LQR design was used in an approach similar to Gavrilets et al. (2004). It is based on the Euler angles representation of the system. Slow/fast decomposition of the dynamics and knowledge of our pilot were used to sketch the values of the weighting matrices. This controller successfully stabilizes the helicopter in hovering flight. Typical results are presented in Figure 13. During this 5 minutes autonomous flight, the position error remains within a three dimensional cylinder which is 1 m high and had a 3 m radius. This flight was obtained outdoor, under 20 km/h wind conditions. The variance of the error approximately equals 1 m in ground position, which is close to GPS error. In the vertical direction, the error variance is below 1m vertically which is close to the absolute barometer error. For velocities, the Variance of error is around 0.75 m.s^{-1} horizontally, and 0.5 m.s^{-1} vertically. Angular error remains within 3 deg in roll and pitch and 15 deg in heading. We feel that these results can be improved upon, especially by tuning the controller further. Most importantly, they represent a first step towards future developments which will incorporate forward motions, and trajectory following techniques (see e.g. Murray et al. (2003)).

Acknowledgement The authors wish to thank Gaël Desilles from DGA for his full technical and scientific support, and Johann Forgeard from DGA for his expert piloting skills.

REFERENCES

P. Abbeel, A. Coates, M. Quigley, and A. Y. Ng. An application of reinforcement learning to aerobatic helicopter flight. *NIPS 19*, 2007.

G. J. Balas. *Flight Control Law Design : An Industry Perspective in Fundamental Issues in Control.* Special issue of European Journal of Control, 2003.

V. Gavrilets, B. Mettler, and E. Feron. Human-inspired control logic for automated maneuvering of miniature helicopter. *Journal of Guidance, Control, and Dynamics*, 27(5):752–759, 2004.

P. Lefort and J. Hamann. *L'hélicoptère.* Chiron, 2e edition., 1988.

B. Mettler. *Identification Modeling and Characteristics of Miniature Rotorcraft.* Boston : Kluwer Academic Publishers, 2003.

B. Mettler, M. B. Tischler, and T. Kanade. Attitude control optimization for a small-scale unmanned helicopter. In *AIAA Guidance, Navigation and Control Conference*, 2000a.

B. Mettler, M. B. Tischler, and T. Kanade. System identification of a model-scale helicopter. Technical Report CMU-RI-TR-00-03, Carnegie Mellon University, january 2000b.

B. Mettler, M. B. Tischler, and T. Kanade. System identification modeling of a small-scale unmanned helicopter. *Journal of the American Helicopter Society*, October 2001.

Motorola. MPC555 / MPC556 user's manual. User's manual, Motorola, 2000.

R. M. Murray, J. Hauser, A. Jadbabaie, M. B. Milam, N. Petit, W. B. Dunbar, and R. Franz. Online control customization via optimization-based control. In T. Samad and G. Balas, editors, *Software-Enabled Control, Information technology for dynamical systems*, pages 149–174. Wiley-Interscience, 2003.

A. Y. Ng, A. Coates, M. Diel, V. Ganapathi, J Schulte, B. Tse, E. Berger, and E. Liang. Inverted autonomous helicopter flight via reinforcement learning. In *International Symposium on Experimental Robotics*, 2004.

G. D. Padfield. *Helicopter Flight Dynamics.* Blackwell Publishing, 2007.

R. W. Prouty. *Helicopter Performance, Stability, and Control.* Malabar : Krieger Publishing Company Inc., 2003.

K. V. Rozhdestvensky. *Aerodynamics of a Lifting System in Extreme Ground Effect.* 1st Edition, Springer-Verlag, 2000.

B. Mettler V. Gavrilets and E. Feron. Nonlinear model for a small-size acrobatic helicopter. In *AIAA Guidance, Navigation and Control Conference*, 2001.

M. A. Dahleh V. Gavrilets, A. Shterenberg and E. Feron. Avionics system for a small unmanned helicopter performing agressive maneuvers. In *19th Digital Avionics Systems Conferences*, 2000.